Preliminary Numerical Tests of the Modification of Mesoscale Convective Systems

J. M. FRITSCH AND C. F. CHAPPELL

Environmental Research Laboratories, NOAA, Boulder, CO 80303

(Manuscript received 2 June 1980, in final form 1 May 1981)

ABSTRACT

A fine-mesh 20-level, primitive equation model is used as a tool for preliminary study of the potential for modification of mesoscale convective systems. The governing system of the model is hydrostatic with the non-hydrostatic convective components parametrically introduced through a convective cloud model subroutine. Two modification possibilities are tested: 1) dynamic seeding, and 2) alteration of the timing and location of initial convection.

Results of artificially changing the time and location of initial convection indicate that the evolution, structure, dynamics and precipitation of mesoscale systems are sensitive to the location where the initial convection happens to develop. Changing the time and location of initial convection may also substantially alter the location and significance of subsequent severe weather as well as potentially beneficial rainfall.

For *idealized* dynamic seeding (i.e., freezing occurs at −10°C in *all* cloud updrafts), model results suggest that seeding enhances convective precipitation and strengthens the dynamics of the mesoscale system. Although mesoscale convergence is increased by the additional latent heat release, the most promising link to additional precipitation seems to be through the enhancement of new growth by strengthening or accelerating moist downdrafts and their associated mesohigh outflow.

1. Introduction

Over the past 30 years, much effort has been expended in attempts to modify convective clouds (see, e.g., Kraus and Squires, 1947; Braham *et al.*, 1957; and Simpson, *et al.*, 1975). On the other hand, very little effort has been directed at modification of mesoscale convective cloud *systems*. This is probably because of the extreme complexity of convective cloud systems, the overwhelming costs of mesoscale field experiments, and the absence of a clear rationale on which to base modification attempts.

In this paper a fine-mesh 20-level, primitive equation model (Fritsch and Chappell, 1980b) is used as a tool for preliminary study of the potential for modification of mesoscale convective systems. The governing system of the model is hydrostatic with the non-hydrostatic convective components parameterically introduced through a convective cloud model subroutine. Two modification possibilities are tested: 1) dynamic seeding, and 2) alteration of the timing and location of initial convection. For each of these two modification treatments, two simulations with identical conditions (Fritsch *et al.*, 1980) were run on a 400 km × 400 km domain with 20 km horizontal resolution. A complete description of the initial conditions is available in Fritsch and Chappell (1980b). In each simulation, the model tests for deep moist convection at all grid points and at every time step. Successive 100 mb layers of air (starting with the layer adjacent to the surface) are first mixed and then lifted to their condensation level where they are checked to determine if the parcel can reach its level of free convection (LFC). Whether or not the LFC is reached depends upon the strength of local eddies or perturbations. In the model it is assumed that the subcloud layer is comprised of a spectrum of perturbations, some of which (probably the largest few) produce clouds. In many instances the environment is conditionally unstable so that deep convection does not occur until these local perturbations grow strong enough to push through an inversion or stable layer. Sometimes, parcels may actually be colder than their environment at their lifting condensation level (LCL), but still have enough upward momentum to overcome negative buoyancy and reach their LFC. Thus, both thermal and momentum components of perturbations should be included in a model test for convective instability. Further, Chen and Orville (1980) have recently shown that perturbations are larger and stronger when low-level convergence (i.e., upward motion) is present. Therefore, local perturbations should reflect not only terrain and heating inhomogeneities, but also the changes in strength due to synoptic and/or mesoscale forcing.

The following formulation for quantifying the maximum size of the local perturbations combines both the thermal and momentum components into a single test. Specifically, deep convection cannot occur in the model unless

$$T_p' > T_e, \tag{1}$$

where T_e is the temperature of the environment at the parcel's LCL, and T_p' an "adjusted" parcel temperature defined by

$$T_p' = T_p + \Delta T. \tag{2}$$

In (2), T_p is the temperature of the parcel at the LCL and ΔT is an assigned perturbation. This perturbation changes according to

$$\Delta T = k_1 + k_2 w^{1/3}, \tag{3}$$

where k_1 is a prescribed constant for each grid element, k_2 is a unit number with dimensions °C $cm^{-1/3}$ $s^{1/3}$, and w is the numerical model vertical motion (in cm s^{-1}) at the LCL. The constant k_1 defines the largest perturbation that would occur when the vertical motion at the top of the boundary layer is zero. Increasing k_1 in the model can be interpreted as an adjustment of the perturbation spectrum to cause larger perturbations. Such an adjustment could be artificially introduced, for example, by dispersing carbon black over a suitable surface area or within a volume of boundary-layer air. The second term in (3) allows the strength of the local perturbations to increase or decrease if the forcing in the model grid element increases or decreases, respectively. For example, if k_1 is assumed to be 1°C, and if the model vertical motion is 1.0 cm s^{-1}, ΔT is 2.0°C; for 10.0 cm s^{-1} lifting, ΔT becomes 3.15°C.

Following a brief description of the mesoscale model in Section 2, Section 3 compares a "control" simulation of the development and evolution of a convective complex to a simulation where the timing and location of initial convection are adjusted by altering ΔT in (2). Aside from the changes in time and location of initial convection, all other conditions in the model simulations are kept the same.

Section 4 compares two simulations where the only difference is that condensate in all convective cloud updrafts is assumed to freeze at −25°C in one case, and at −10°C in the other. Section 5 discusses the results of the two modification treatments.

2. Mesoscale numerical model

The primary model characteristics and convective parameterization assumptions are listed below. A complete description is available in Fritsch and Chappell (1980a,b).

a. Numerical model characteristics

1) The conservation of momentum equations are cast in the primitive equation flux form.

2) Height is the vertical coordinate with 20 constant height levels defined at the climatological mean heights of significant pressure levels (i.e., every 50 mb).

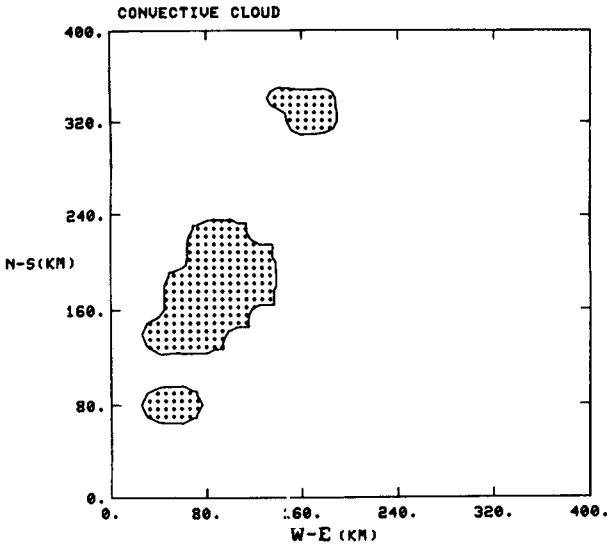

FIG. 1. Location of active convection 0.5 h following the onset of deep convection in the control simulation.

3) The horizontal domain is 400 km on a side with a 20 km grid mesh. Both the domain and mesh are arbitrary.

4) Detailed surface topography is not included.

5) Lateral boundaries are periodic at the east and west and constant at the north and south. A "sponge" condition is applied to the prognostic tendencies along the north and south boundaries.

6) The upper boundary condition requires the vertical motion to be zero or $dz/dt = w = 0$.

7) The lower boundary condition includes a surface drag with linear drag decrease through the transition layer, also, $w = 0$.

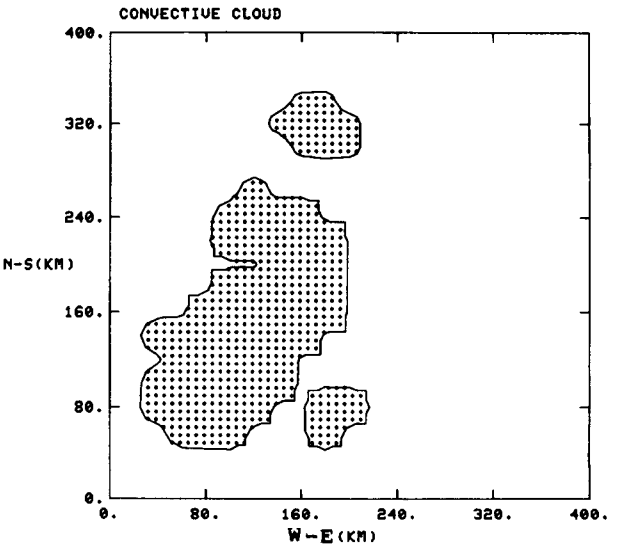

FIG. 2. As in Fig. 1 except at 1.0 h.

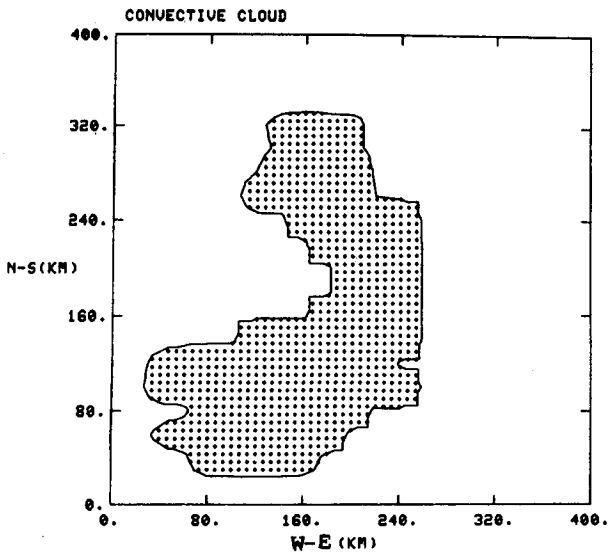

FIG. 3. As in Fig. 1 except at 1.5 h.

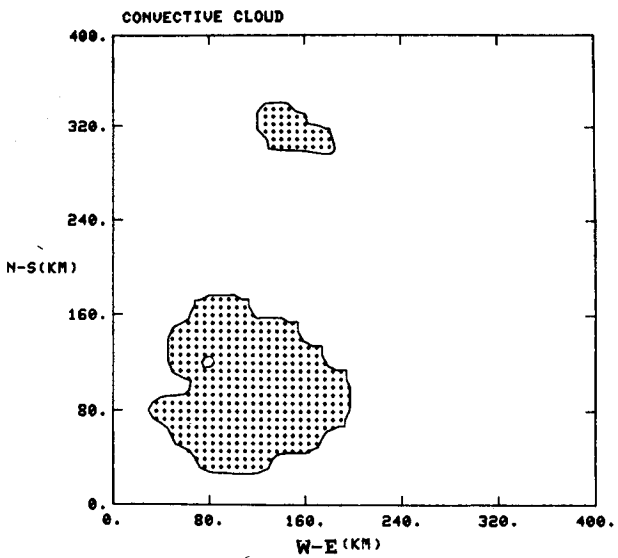

FIG. 5. Location of active convection 0.5 h following the onset of deep convection in the modified simulation.

8) The finite-difference formulations are centered in time and space, and a time filter is included to avoid "separation of solutions". Time steps are 30 s.

9) A horizontal diffusion filter, applied as a smoother-desmoother, is used to help control numerical and boundary generated noise.

10) Vertical temperature and density adjustments have been neglected except in the moist convective calculations.

11) The governing system of equations is hydrostatic with non-hydrostatic effects included through the convective parameterization. Pressure u and v components of the wind, and mixing ratio, are the prognostic variables while temperature is diagnosed hydrostatically, and density is derived through the gas law. Vertical motion is diagnosed using Richardson's equation.

b. Convective parameterization assumptions and constraints

1) Moist convection only occurs when air is forced to its level of free convection (i.e., when potential buoyant energy becomes available).

2) Mass transports by moist convection are closely approximated by a model cloud ensemble which treats *deep* convection as the dominant cloud form.

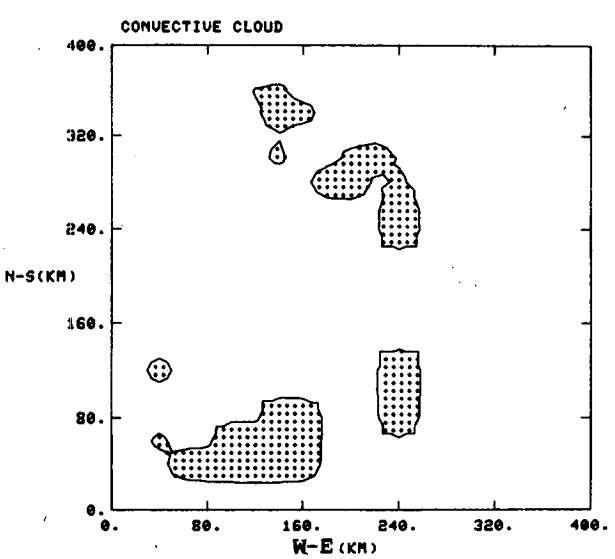

FIG. 4. As in Fig. 1 except at 2.0 h.

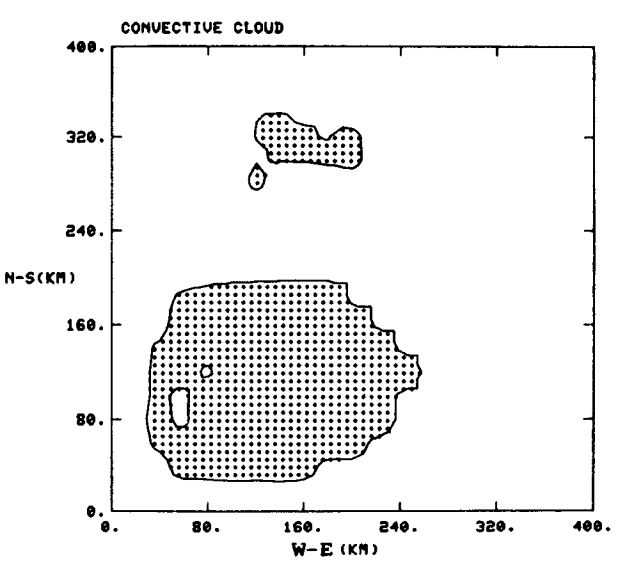

FIG. 6. As in Fig. 5 except at 1.0 h.

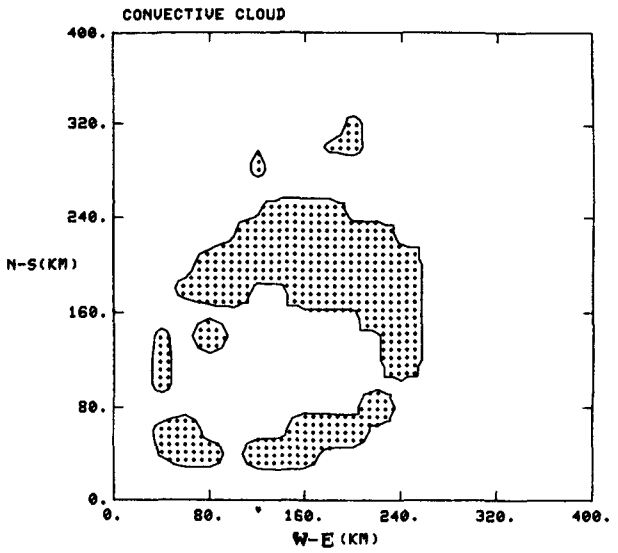

FIG. 7. As in Fig. 5 except at 1.5 h.

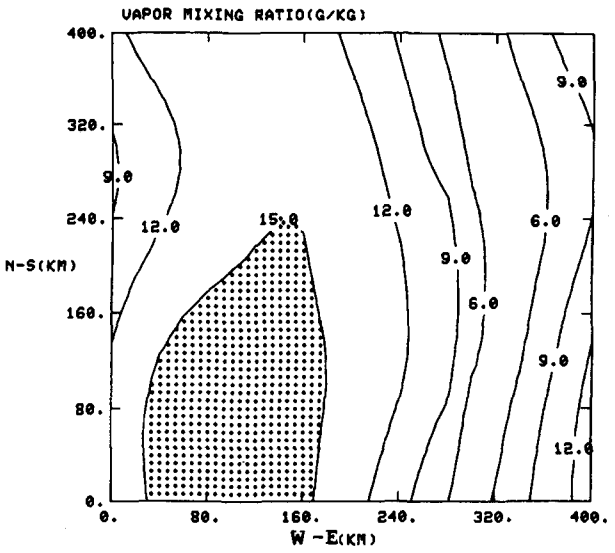

FIG. 9. Surface water vapor mixing-ratio pattern 0.25 h following the onset of deep convection in the modified simulation. Shaded area indicates mixing-ratios > 15 g kg^{-1}.

3) Precipitation efficiency of the convective clouds is inversely proportional to the vertical wind shear across the cloud depth.

4) The grid-scale stabilization rate [destruction of Available Buoyant Energy (ABE)] by moist convective processes is equivalent to minus the model generated ABE divided by the estimated time for the convective "cells" to move across the grid element. This time period τ_c, is obtained by dividing the grid length by the mean environmental wind speed over the cloud depth; τ_c has a lower limit defined by the average lifetime of individual cells (30 min), and an upper limit (one hour) to allow large-scale changes to alter the characteristics of the convective clouds. If the period of time necessary to consume all of the ABE is greater than 1 h, the computed rate of stabilization is still applied for 1 h, even though all the ABE will not be consumed. After an hour, the atmosphere is again checked for instability and convection may be initiated once again (at different adjustment rates, however).

5) The vertical distribution of the convective heating and cooling of environmental air is the resultant structure that occurs when:

(i) The cloud-model processes sufficient mass to

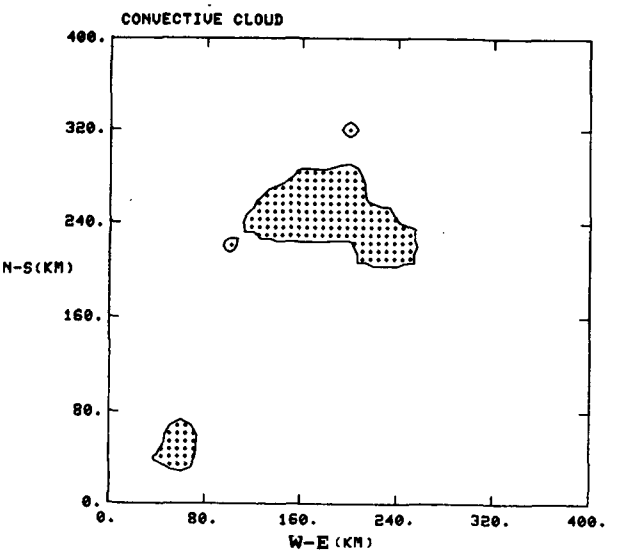

FIG. 8. As in Fig. 5 except at 2.0 h.

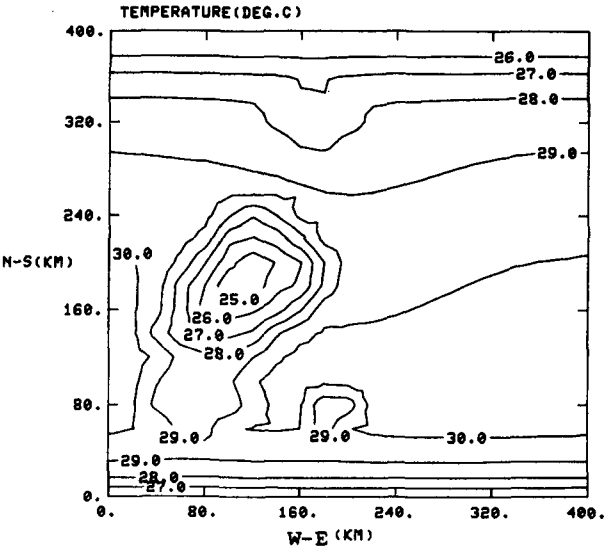

FIG. 10. Surface temperature pattern at 1.0 h following the onset of deep convection in the control simulation.

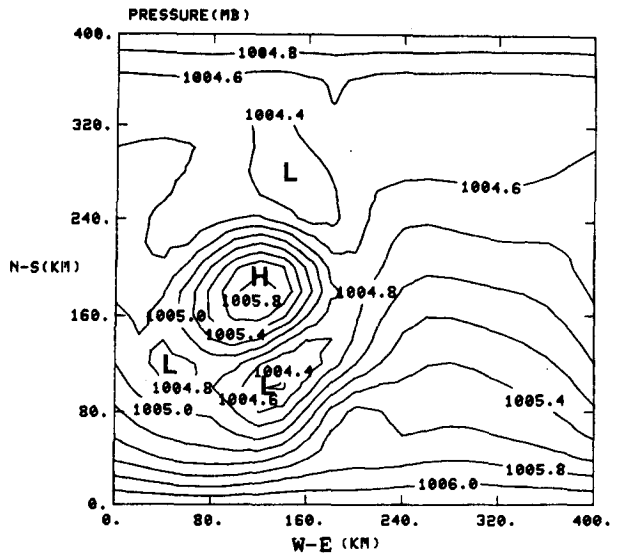

FIG. 11. Surface pressure pattern at 1.0 h following the onset of deep convection in the control simulation.

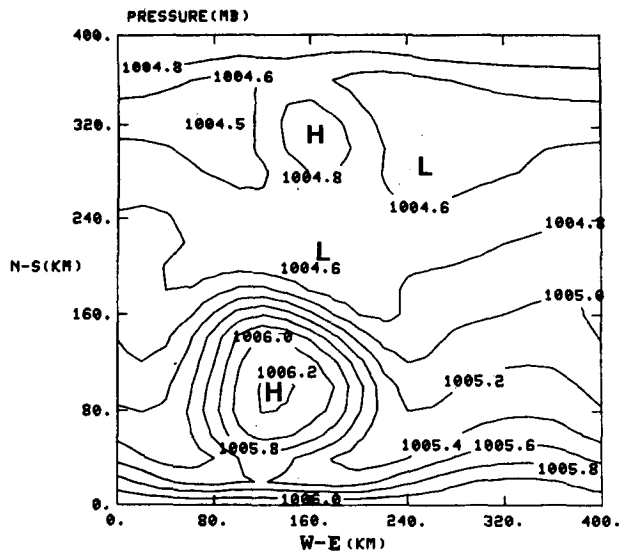

FIG. 13. Surface pressure pattern at 1.0 h following the onset of deep convection in the modified simulation.

produce the net stabilization by moist convection as specified in 4) above.

(ii) The environmental vertical motion field adjusts to the mass requirements of the convective cloud model and the larger scale vertical transports.

6) The changes in temperature and mixing ratio at a model grid point are the sum of the effects of compensating subsidence in the environment plus the effect of area-weighting the cloud updraft, downdraft, and environment. Also, when deep convection is active within a particular grid element, radiational heating (or cooling) at the surface is terminated until convection ceases within that element.

7) Momentum is vertically exchanged through bulk mixing processes in the cloud updrafts and downdrafts and by compensating environmental vertical motions.

The effects of the convective processes on the mesoscale are gradually fed into the governing system of equations. Changes are linearly introduced over the period of time defined by τ_c. Temperature

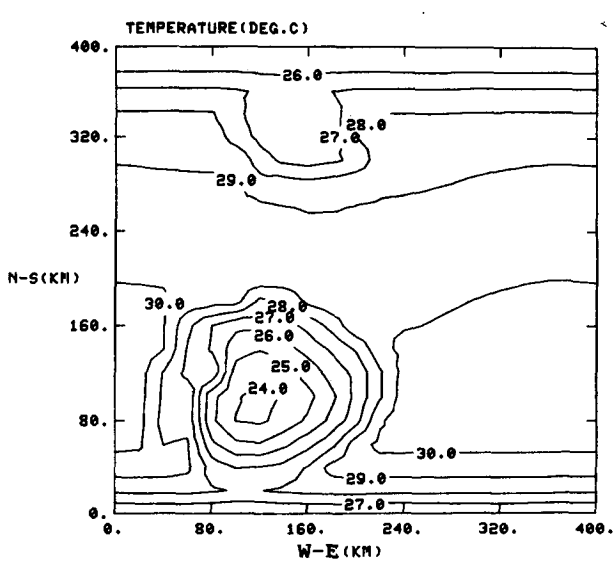

FIG. 12. Surface temperature pattern at 1.0 h following the onset of deep convection in the modified simulation.

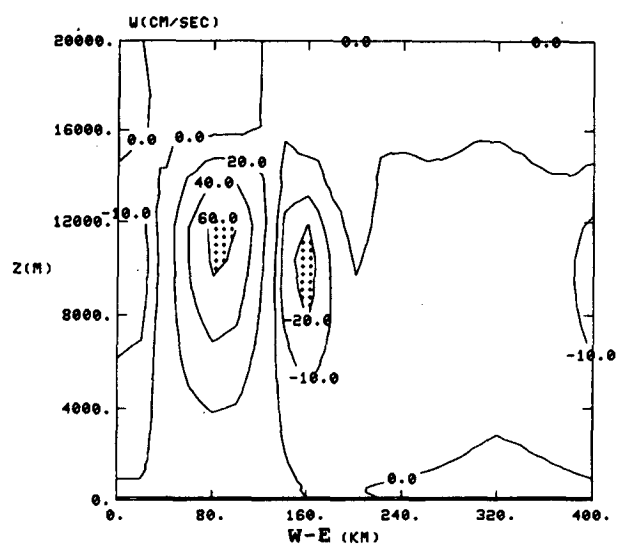

FIG. 14. East-west vertical cross section of vertical motion at 1.0 h following the onset of deep convection in the control simulation. Section taken at 100 km north of origin of domain (see Fig. 2). Shaded areas indicate ascending motions > 60 cm s^{-1} and descending motions > 20 cm s^{-1}.

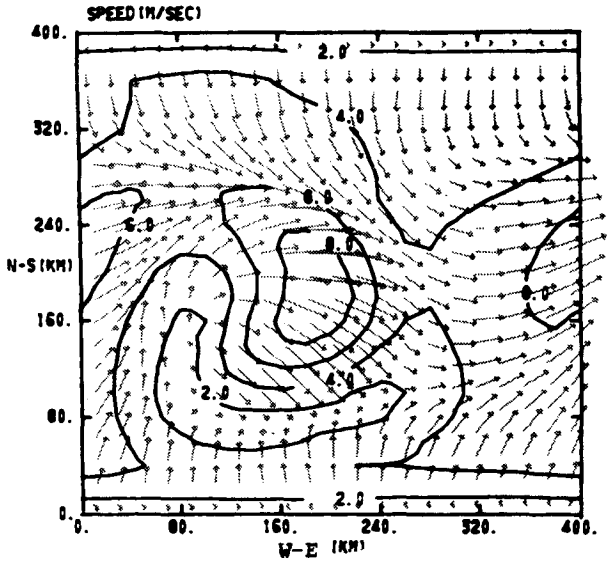

FIG. 15. Surface streamline (arrows) and isotach pattern at 1.5 h following the onset of deep convection in the control simulation.

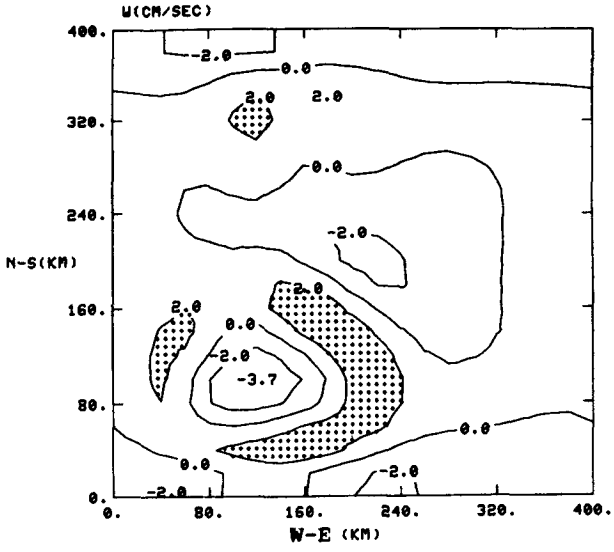

FIG. 17. As in Fig. 16 except at 1.0 h following the onset of deep convection in the modified simulation. Shaded areas indicate ascending motion > 2 cm s^{-1}.

changes are incorporated into the governing system through heating terms which appear in the pressure tendency and vertical motion equations.

3. Alteration of timing and location

Figs. 1–4 show the evolution of convection during the control simulation. Figs. 5–8 show a significantly different evolution which resulted from only a slight change in k_1 in (3). In the control run k_1 was −0.25°C, while in the modified run k_1 was set to zero, i.e., ΔT's in (2) were slightly larger in the modified run. As a result, parcels of air were able to more quickly reach their level of free convection so that the time of initial deep cloud development was ~30 min sooner in the "modified" simulation (i.e., 2.5 h into the modified simulation versus 3.0 h for the control). Also, notice that the *main* area of convection in the control case developed in the west-central part of the domain (Fig. 1) while in the modified simulation it formed in the southwest quadrant close to the

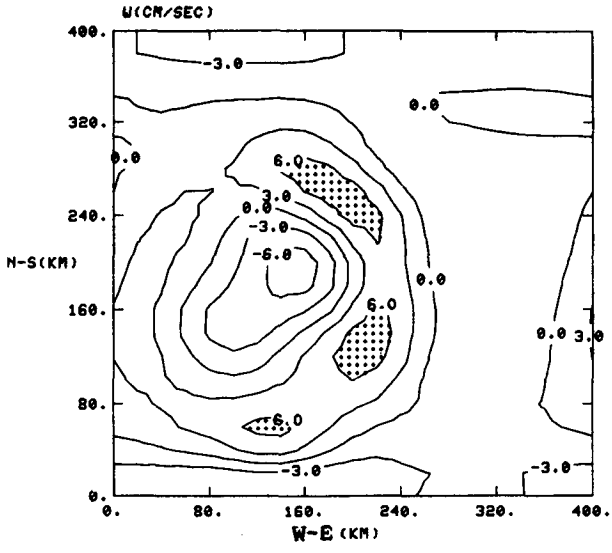

FIG. 16. Vertical motion pattern at z = 0.988 km (~900 mb level) at 1.5 h following the onset of deep convection in the control simulation. Shaded areas indicate ascending motion > 6 cm s^{-1}.

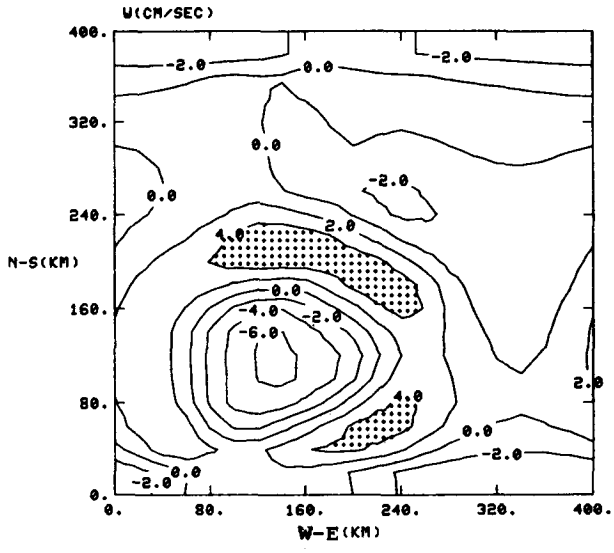

FIG. 18. As in Fig. 16 except at 1.5 h following the onset of deep convection in the modified simulation. Shaded areas indicate ascending motion > 4 cm s^{-1}.

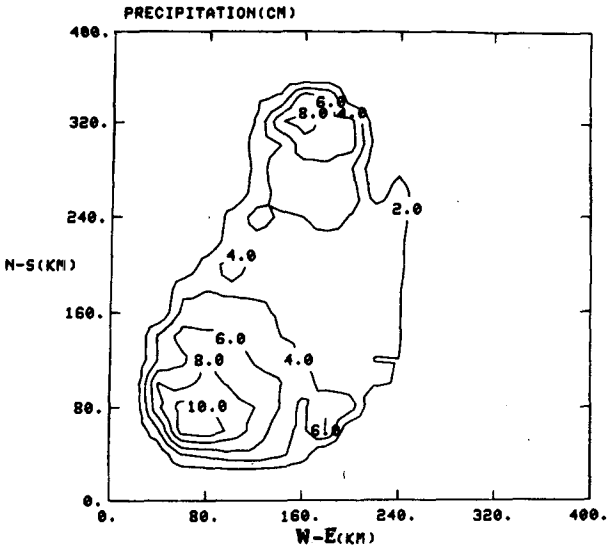

FIG. 19. Total precipitation after 2 h of convection in the control simulation.

moisture source (see Figs. 5 and 9). Furthermore, the control case generated more of a line-type structure compared to the nearly circular system that formed in the modified simulation. These differences in how the convection evolved are strongly reflected in the surface pressure and thermal fields. In each case, the strongest boundary-layer cooling and associated mesohigh developed in an area nearly coincident with the main area of convection (cf. Figs. 1, 10 and 11 to 6, 12 and 13). In addition to the shift in the position of the mesohigh, the locations of the mesolows were significantly different in the two simulations. In the control case, two mesolows developed south of the mesohigh, while in the modified case all mesolows are north of the main mesohigh. The positions of the mesolows and the evolution of the convection are closely tied to two types of direct vertical circulations which develop in response to the convection. One type is a rather deep circulation centered over the area of active convection and extending into the lower stratosphere (Fig. 14). This circulation develops in response to the upper tropospheric compressional warming of the environment by the thunderstorms. The subsidence portion of this circulation is sometimes responsible for mesocyclogenesis (see Hoxit *et al.*, 1976; Fritsch and Chappell, 1980) while the ascending portion enhances middle and low-level convergence into the convective system. The second type of vertical circulation is strictly a low-level phenomenon associated with the convergence along the mesohigh outflow. Figs. 15 and 16 show the surface outflow from the mesohigh and the vertical motion at ~900 mb, respectively, at 1.5 h following the onset of deep convection in the control simulation. For both cases, a comparison of the evolution of the convectively driven vertical circulations suggests that the subsidence portion of the deep circulation suppresses convection until the low-level forcing from the outflow arrives and reverses the suppressed conditions. If convection can be enhanced to develop sooner in one area, it may very well suppress convection that may have naturally developed in an adjacent area. *Thus, the convection itself plays a major role in determining the details of the convective system* (cf. Figs. 17 and 18 to 5 and 6).

Figs. 19 and 20 show the total precipitation after 2 h of convection for both the control and modified simulations, respectively. The average precipitation over the entire domain was 18% less in the modified case than in the control case. Examination of the evolution and distribution of the precipitation in the two convective systems indicates at least two possible reasons for the difference in average precipitation. First of all, in both model runs, convection was not permitted to occur at or move through the northern or southern boundaries. Thus, for the modified case, it can be argued that the close proximity of the southern boundary to the mesohigh may have artificially limited the mesohigh outflow and therefore limited the southern movement of the mesosystem as well. If this is true, the *total area* of precipitation (and therefore total precipitation) may have been larger in the modified case if the domain had been expanded. On the other hand, the southern boundary also restricted southern movement in the unmodified case, but to a slightly lesser extent (cf. Figs. 19 and 20).

More significant than the possible impact of the southern boundary, however, is that throughout the

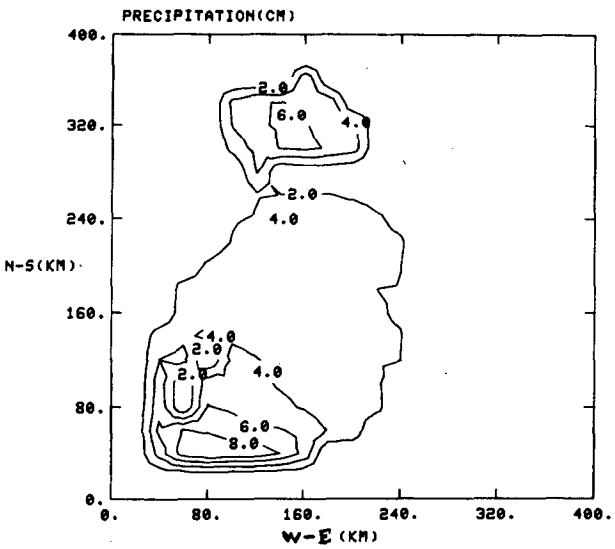

FIG. 20. Total precipitation after 2 h of convection in the modified simulation.

model domain, precipitation amounts were generally less in the modified case than in the control. This likely occurred because *more buoyant energy was available for convection in the control simulation.* That is, heating in the boundary layer continued 30 min longer in the control run than in the modified run before deep convective clouds developed. Thus, control-run clouds were larger, moist downdrafts were stronger, and more mass and water vapor were processed to produce more precipitation. Further, had the model domain been larger, it is likely that the stronger low-level forcing from the stronger moist downdrafts in the control simulation (cf. Figs. 16 and 18) would have further accentuated the differences between the two simulations by producing a larger *area* of precipitation in the control run. In general, though, the results suggest that the distribution of precipitation is sensitive to the initial timing and configuration of convection.

4. Dynamic seeding

Dynamic seeding is based on the theory that massive artificial ice nucleation in updraft regions increases buoyancy through a net release of the heats of fusion, deposition, and condensation, thereby producing taller, wider and longer lasting clouds (Simpson *et al.*, 1965). Since larger, longer lasting clouds process more water, it is postulated that seeded clouds should produce more rain than their unseeded counterparts. In an attempt to test the sensitivity of a convective cloud complex to dynamic seeding, two simulations, one a control and the other "seeded", were run starting from identical initial conditions. In the "seeded" simulation, massive artificial ice nucleation is simulated by introducing freezing in all cloud updrafts at −10°C instead of −25°C (unseeded). Thus, the seeded updraft parcels experience greater latent heat release than the unseeded. Fig. 21 shows the thermodynamic paths of seeded and unseeded parcel ascent at point *P* in Fig. 23. The difference in potential buoyant energy (indicated by the shaded area on the thermodynamic diagram) when freezing is introduced at −10°C instead of −25°C is ~10%. Similar parcel paths and differences in buoyant energy occurred at other grid points where deep convection developed. This increase in buoyant energy is manifested as stronger vertical motions and therefore larger clouds. (The increase in cloud-top height is not included in Fig. 21). Also, as a consequence of the increase in buoyant energy, the convective parameterization permits additional convective overturning in each grid element so that the total

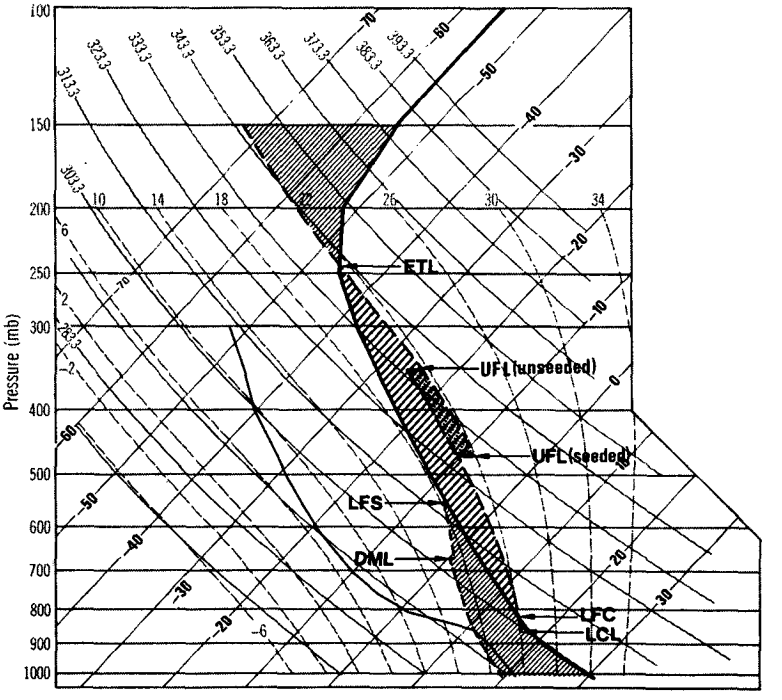

FIG. 21. Upper air sounding and thermodynamic paths of parcel ascent for seeded and unseeded parcels. Thermodynamic paths are for a lifted parcel [at point P (Fig. 23)] with mean thermodynamic characteristics of lowest 100 mb layer. LCL is the lifting condensation level, LFC the level of free convection, DML the moist downdraft melting level, LFS the level of free sink, UFL the updraft freezing level, and ETL the parcel equilibrium temperature level.

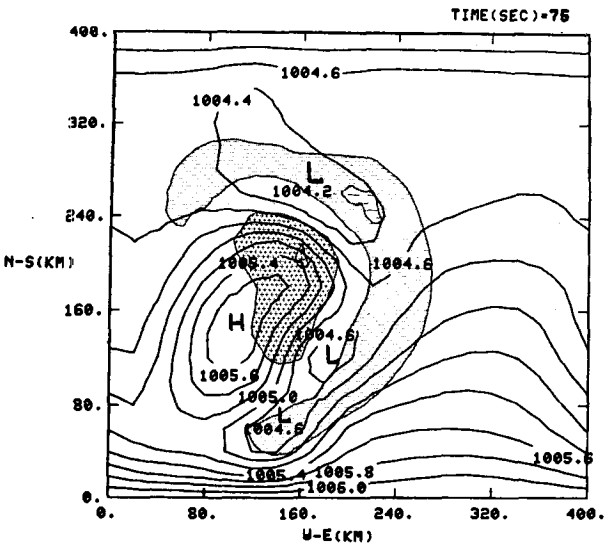

FIG. 22. Unseeded-run surface pressure [solid lines (mb)] and pressure differences between seeded and unseeded runs (shaded areas). Area shaded with small minus signs indicates a pressure difference of at least −0.2 mb while the area shaded with small plus signs indicates differences of at least +0.2 mb. Large plus and minus signs indicate pressure differences of ±0.4 mb, respectively.

amount of mass ascending in updrafts and descending in moist downdrafts is increased. In all clouds it is assumed that no condensate initiates its fall from below the freezing level, i.e., no "warm cloud" processes are permitted. It also is assumed that the buoyancy impulse at the freezing level is communicated to the updraft air below. Specifically, it is assumed that the buoyancy acceleration of the parcel causes a pressure fall in the layer of air below the freezing level. This results in additional low-level mass and moisture convergence to feed the growth of the cloud.

Comparison of the two integrations revealed several obvious differences. First, the seeded convective complex generated stronger mesoscale pressure systems . . . deeper mesolows and higher mesohighs. For example, the unseeded surface pressure field, superimposed on the pressure difference between seeded and unseeded cases, is shown in Fig. 22.[1] The large crescent-shaped area shaded with small "minus" signs is where the seeded surface pressure is 0.2 mb lower than the unseeded case. Seeded surface pressures were 0.2 mb higher in the area shaded with small plus signs. Areas shaded with the large plus or minus signs indicate pressure differences of ±0.4 mb, respectively. At the end of the numerical integration, when almost all of the convection had dissipated, the seeded mesohigh was ~0.25 mb higher than the unseeded high and the seeded mesolow was ~0.5 mb lower than the unseeded low. The more intense mesohigh appeared to be the result of stronger moist downdraft cooling. For example, Fig. 23 shows the moist downdraft cooling (°C h^{-1}) for the unseeded case superimposed on the cooling rate difference (shaded areas) between seeded and unseeded runs. Note the large area where the seeded moist downdraft cooling rate is 2°C h^{-1} stronger than the unseeded case. While the mesohigh was strengthened by changes at low levels, the deeper mesolows appeared in conjunction with stronger meso-β scale subsidence circulations aloft. At times seeded case subsidence is over 5 cm s^{-1} stronger than the unseeded case. Mesoscale ascent in the seeded case exceeds the non-seeded by over 20 cm s^{-1} (see Fig. 24). Further evidence that seeding strengthened the mesosystem is the stronger mesohigh outflow and enhanced lifting just ahead of the outflow boundary (see Fig. 25). Seeded outflow is as much as 3 m s^{-1} stronger than unseeded outflow. Correspondingly, vertical motion along the outflow boundary increased by over 2 cm s^{-1}.

Part of the differences shown in Fig. 22 result from more rapid *propagation* of the seeded system. This is a consequence of more intense cooling by the moist downdrafts and the associated mechanical lifting along the downdraft outflow boundaries. Some measure of the influence of the faster propagation shows up in the precipitation fields. For example, Fig. 26 shows the unseeded precipitation superimposed on the precipitation difference at 75 min after convection began. Note that the difference

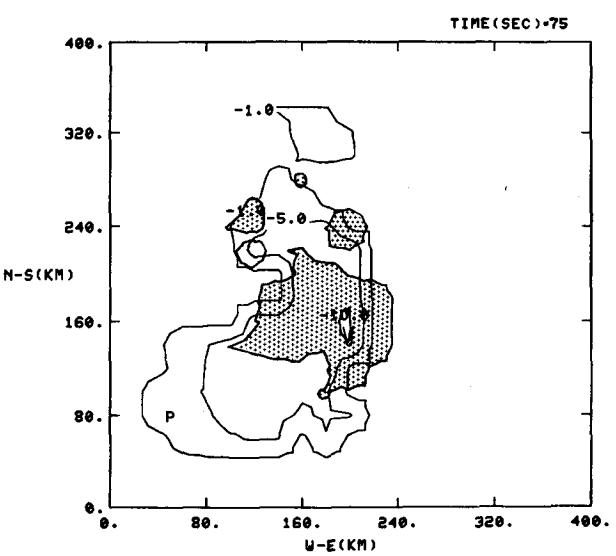

FIG. 23. Unseeded-run moist downdraft cooling rate [solid lines (°C h^{-1})] at the surface and cooling rate difference between seeded and unseeded runs (shaded areas). Areas shaded with plus and minus signs indicate seeded run cooling rates at least 2°C h^{-1} stronger or weaker, respectively, than unseeded rates.

[1] For Figs. 22–27 the time shown at the top right-hand corner is "minutes following the onset of deep convection."

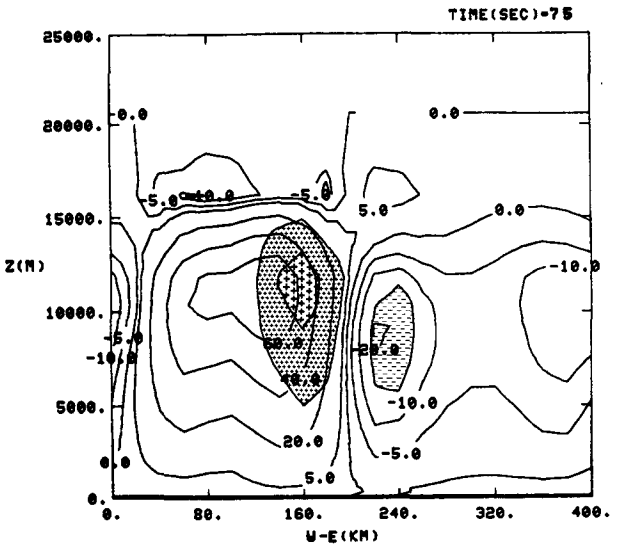

FIG. 24. East–west vertical cross section of seeded-run vertical motion [solid lines, (cm s^{-1})] and vertical motion differences between seeded and unseeded runs (shaded areas). Area shaded with small minus signs indicates seeded-run subsidence over 5 cm s^{-1} stronger than unseeded-run subsidence. Small and large plus signs indicate seeded-run upward vertical motion 10 and 20 cm s^{-1} larger, respectively, than unseeded-run vertical motion. Cross section taken at 100 km north of origin of domain (see Fig. 23).

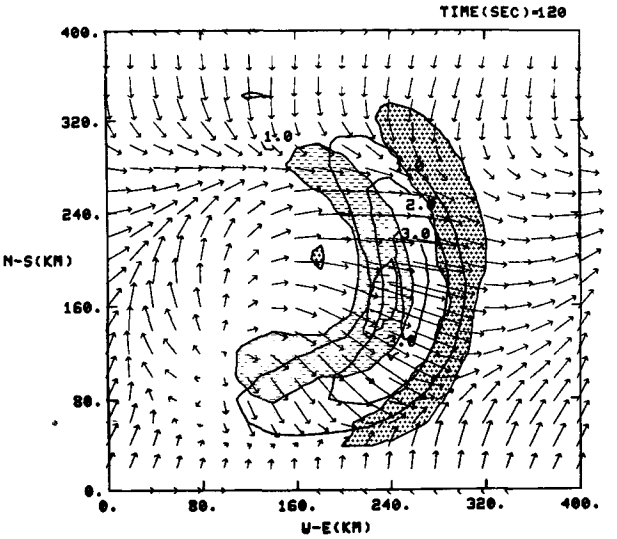

FIG. 25. Seeded surface wind pattern (arrows), speed difference (m s^{-1}) between seeded and unseeded runs (solid lines), and 0.988 km (~900 mb level) vertical motion difference (shaded areas) between seeded and unseeded runs. Areas shaded with small plus or minus signs indicate seeded run vertical motions 2 cm s^{-1}, greater or less, respectively, than unseeded run. Large minus signs indicate area of subsidence in seeded run 4 cm s^{-1} stronger than unseeded run.

pattern extends well to the east of the unseeded 1 cm contour. At this time, the seeded precipitation exceeds the unseeded precipitation by 24% when averaged over the entire domain. In the next 45 min, however, the seeded system slows down as it runs out of low-level moisture and the unseeded system catches up. Fig. 27 shows the cumulative unseeded precipitation superimposed on the precipitation difference at 2 h following the onset of convection. The seeded precipitation now exceeds the unseeded by only 15%. Also, note that the largest differences are usually along the periphery of the precipitation region suggesting that the increases in precipitation come primarily from increasing the area of convection.

5. Summary and discussion

Preliminary numerical studies of artificially changing the time and location of initial convection in a convectively unstable environment indicate that the evolution, structure, dynamics and precipitation of the mesoscale convective system may be sensitive to the time and location where the initial convection happens to develop. Further, since mesocyclogenesis appears to be dependent on the configuration of convective elements (see Fritsch and Chappell, 1980b), and since mesolows have been documented as having a correlation with severe storms (Magor, 1958), changing the initial time and location of convection may substantially alter the location and significance of subsequent severe weather as well as potentially beneficial rainfall.

For *idealized* dynamic seeding (i.e., freezing occurs at −10°C in *all* cloud updrafts), the numerical model results suggest that seeding enhances convective precipitation and strengthens the dynamics of the mesoscale system. Although mesoscale convergence is increased by the additional latent heat release, the most promising link to additional precipitation seems to be the enhancement of new growth by strengthening mesohigh outflow. Specifically, seeding techniques might do well to focus on enhancing moist downdraft outflow and the associated lifting that initiates new cloud growth. If the mesohigh outflow can be strengthened, the prospects for "new growth" may be significantly enhanced, particularly on days where large-scale forcing is weak or neutral. Although one may argue whether or not seeding strengthens individual moist downdrafts, simply accelerating the life cycle of natural new growth may lead to more downdraft mass per unit time and therefore stronger mesohighs, outflows, lifting, etc. Furthermore, mesohighs often have well-defined boundaries and thermodynamic characteristics. Thus, it may be simpler to document seeding-induced changes to mesohighs rather than trying to establish differences in a laterally unbounded deeper mesoscale circulation that redistributes latent heat effects in a much more nebulous manner.

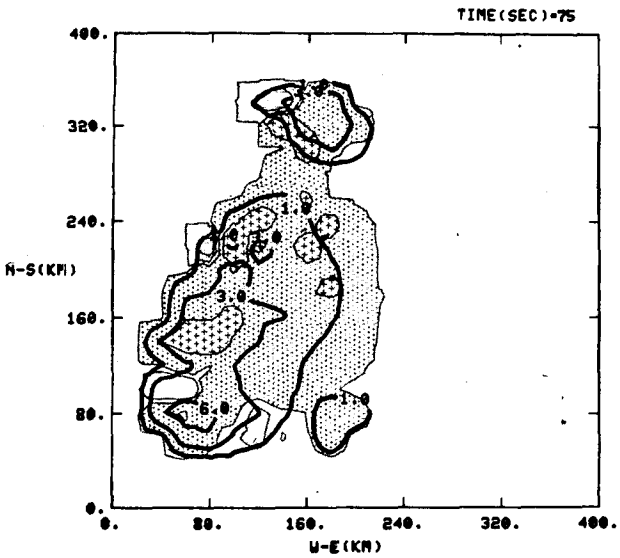

FIG. 26. Cumulative unseeded-precipitation [dark solid lines (cm)] and precipitation difference between seeded and unseeded runs (shaded areas) at 75 min following the onset of convection. Areas shaded with small plus or minus signs indicate seeded precipitation 0.1 cm greater or less, respectively, than unseeded precipitation. Large plus or minus signs indicate precipitation differences of ±1.0 cm, respectively.

From a practical standpoint, it is interesting to consider the possibility of field attempts to modify *mesoscale* convective *systems*. Whereas it is easy to assume the idealized glaciation that was imposed in the model, the actual introduction of sufficient ice nuclei to cause glaciation at such warm temperatures is another matter. One must not only consider the logistics of introducing seeding material over such a large volume, but some knowledge of the detailed microphysical structure and seeding response of the clouds must be known or anticipated in advance of application. Specifically, the rate of glaciation is strongly modulated by such variables as liquid water content, drop-size distribution, temperature (which determines number of active ice nuclei), type of nucleation, vertical motion, etc. Since the convective parameterization used in the numerical model does not include detailed microphysics, it is difficult to assess the relative roles of several of these cloud parameters. For the particular system simulated by the model, however, appropriate values for some of these parameters have been determined. For example, the average cloud in the model domain has a cloud-base temperature of ~16°C at 850 mb and a corresponding water vapor mixing ratio of 13.5 g kg^{-1}. By the time the entraining updraft parcel reaches the −10°C level, its water vapor mixing ratio has decreased to ~3.5 g kg^{-1} (partly due to condensation and partly to the entrainment of drier air). The liquid water content at the −10°C level, assuming all of the condensate is carried along in the updraft, is ~5.5 g m^{-3}.

The seeding "time window" within which to produce glaciation over, for example, the −5 to −20°C temperature zone, is a function of the mean updraft velocity in this zone. After allowing for the drag of liquid water, the average updraft velocity in this temperature zone is ~20 m s^{-1}. Thus, for the clouds in the model simulation, the seeding "time window" may be as short as 100 s if seeding material is introduced from below.

With these estimates for liquid water content and time available to freeze it, the numerical results of Lamb *et al.* (1981) can be used to estimate the amount of seeding material necessary to glaciate the convective system. Specifically, for a cloud with 5.0 g m^{-3} of liquid water (of which 60% is rainwater) their results suggest that 10–100 nuclei L^{-1} are sufficient to produce about 50–90% of glaciation[2] in 100–200 s, depending on whether deposition or contact nucleation is invoked. Consider now that the convective *system* in the model simulation processes, on the average, ~10^{12} L s^{-1} of cloudy air through the −10°C level. This system would require at least 10^{13} to 10^{14} active nuclei s^{-1} for glaciation. According to Grant and Finnegan (1981), a new ice nuclei generation technique can produce about 10^{13} active nuclei (at −10°C) per 0.5 g of seeding material per minute. This estimate takes into account losses due to solubility, washout, etc. Thus, in order to produce 10^{13}–10^{14} nuclei L^{-1} s^{-1}, anywhere from 60 to 600 generating units processing a total of approximately 30–300 g of seeding material per s (about 10^{2}–10^{3} kg h^{-1}) would be necessary. This is a large

[2] Glaciation is defined as that point in time when the graupel concentration builds up to the time-dependent concentration of rain.

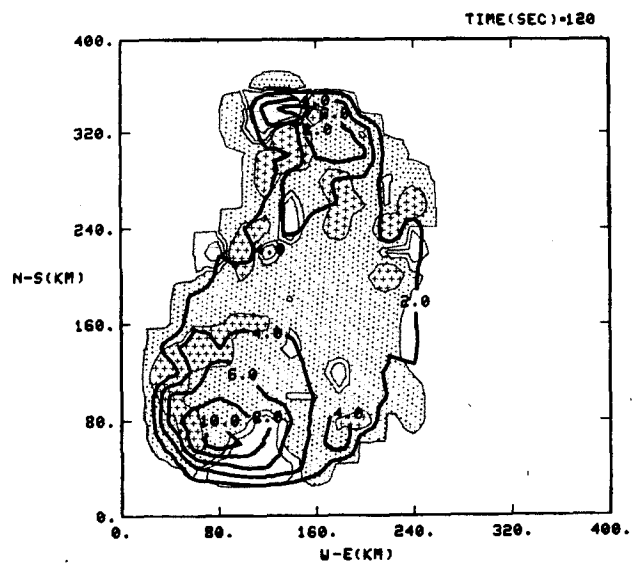

FIG. 27. As in Fig. 26 except for 120 min following onset of convection.

amount of seeding material, but could be delivered within the proper time window by several corporate-jet-type aircraft.

It is important to realize that the above computation is for a convective system that is nearly a "worst case" seeding situation. The potential increase in available buoyant energy is minimal (~10%) and the degree of difficulty in attaining glaciation quick enough to realize this increase in buoyant energy is nearly maximal. On the other hand, numerical simulations by Hsie *et al.* (1980) suggest that glaciation "time windows" (for similar clouds) may be significantly longer—on the order of 3–6 min. Further, in some instances, the addition of the latent heat of fusion can mean the difference between whether or not *deep* convection develops at all. Clearly, in these situations the prospects for early glaciation are considerably enhanced and the potential impact is much more substantial.

Finally, because the above simulations were carried out with a rather crude convective cloud model and on idealized initial conditions over a rather limited domain, caution must be exercised in interpreting the results. Further, little significance should be attached to the *magnitude* of the differences between these simulations—the main thrust of the paper is to stress the qualitative differences, the physical mechanisms which produce them, and the strong nonlinearity of the interactions between convective cloud systems and their environment. In addition to the buoyancy changes which were incorporated in the seeded simulation, other potentially important microphysical changes are likely. Therefore, numerous additional tests on observed convective systems using more sophisticated cloud models (e.g., Orville and Kopp, 1977; Cotton *et al.*, 1980) must be completed before the sensitivity of convection to dynamic seeding and changes in initial time and location can be realistically assessed.

Acknowledgments. The authors thank Fredric N. Gould for his considerable help in completing the numerical simulations and John M. Brown, William O. Cotton and Harold D. Orville for kindly reviewing the manuscript. This work was partially supported by the Bureau of Reclamation, Division of Atmospheric Resources Management. The manuscript was skillfully prepared by Mrs. Elaine Ardourel, Mrs. Irene Bork and Mrs. Serena Kierein.

REFERENCES

Braham, R. R., Jr., L. J. Battan and H. R. Byers, 1957: Artificial nucleation of cumulus clouds. *Meteor. Monogr.*, No. 11, Amer. Meteor. Soc., 47–85.

Chen, C., and H. D. Orville, 1981: Effects of mesoscale convergence on cloud convection. *J. Appl. Meteor.*, **19**, 256–274.

Cotton, W. R., T. Nehrkorn, G. Tripoli and J. B. Cunning, 1980: A three-dimensional simulation of the dynamic response of a Florida cumulus to seeding. *Proc. Third WMO Sci. Conf. Weather Modification*, Clermont-Ferrand, France, Vol. 1, 63–66.

Fritsch, J. M., and C. F. Chappell, 1980a: Numerical prediction of convectively driven mesoscale pressure systems. Part I: Convective parameterization. *J. Atmos. Sci.*, **37**, 1722–1733.

——, 1980b: Numerical prediction of convectively driven mesoscale pressure systems. Part II: Mesoscale model. *J. Atmos. Sci.*, **37**, 1734–1762.

——, E. L. Magaziner and C. F. Chappell, 1980: Analytical initialization for three dimensional numerical models. *J. Appl. Meteor.*, **19**, 809–818.

Hoxit, L. R., C. F. Chappell and J. M. Fritsch, 1976: Formation of mesolows and pressure troughs in advance of cumulonimbus clouds. *Mon. Wea. Rev.*, **104**, 1419–1428.

Hsie, E. Y., R. D. Farley and H. D. Orville, 1980: Numerical simulation of ice-phase convective cloud seeding. *J. Appl. Meteor.*, **19**, 950–977.

Kraus, E. B., and P. Squires, 1947: Experiments on the stimulation of clouds to produce rain. *Nature*, **159**, 489–491.

Lamb, D., R. I. Sax and J. Hallett, 1981: Mechanistic limitations to the release of latent heat during the natural and artificial glaciation of deep convective clouds. *Quart. J. Roy. Meteor. Soc.*, (in press).

Magor, B. W., 1958: A mesolow associated with a severe storm. *Mon. Wea. Rev.*, **86**, 81–90.

Orville, H. D., and F. J. Kopp, 1977: Numerical simulation of the life history of a hailstorm. *J. Atmos. Sci.*, **34**, 1596–1618.

Simpson, J., R. H. Simpson, D. A. Andrews and M. A. Eaton, 1965: Experimental cumulus dynamics. *Rev. Geophys.*, **3**, 387–431.

——, J. C. Eden and A. R. Olsen, 1975: On the design and evaluation of cumulus modification experiments. *J. Appl. Meteor.*, **14**, 946–958.